Kovove Mater. 52 2014 11–17
DOI: 10.4149/km_2014_1_11

Research on laser welding-brazing of dissimilar Mg alloy and stainless steel

Ming Jiang, Ming Gao*, Geng Li, Cheng Zhang, Xiaoyan Zeng

Wuhan National Laboratory for Optoelectronics, Huazhong University of Science and Technology, Wuhan 430074, P. R. China

Received 10 March 2013, received in revised form 10 April 2013, accepted 22 August 2013

Abstract

Laser welding-brazing was developed to join dissimilar AZ31B magnesium (Mg) alloy and AISI304 stainless steel using a high power fiber laser. The maximum joint strength was 211 MPa, which reached 89.8 % of Mg base metal. The interface characterization and fracture behavior of the joints were investigated by employing optical microscopy, scanning electron microscopy, energy-dispersive X-ray spectroscopy, and X-ray diffraction. A transition zone was observed at the interface of fusion zone/steel, where the intermetallic compounds of Mg_2Ni and $Mg_{17}Al_{12}$ were found. The offset from the center of laser beam to the edge of joint seam played a big role in the joining strength by changing the area fraction of reaction layer to whole interface. The smaller the laser offset, the larger the area fraction of reaction layer to whole interface, and thus the stronger the joining strength is. By the characteristics observed on fracture surface, the fracture behavior was summarized.

K e y w o r d s: laser brazing, stainless steel, magnesium alloy, interface, tensile strength

1. Introduction

Steel is currently the widely used metal material of modern industry because of the excellent ductility, strength and low overall component production costs [1]. Magnesium (Mg) alloy has the potential to replace steel and aluminum in many structural applications due to the low density, high specific strength along with good damping capacity [2]. Thus the joining of Mg/steel deserves more attention than ever because it can gather more advantages in one part [3, 4]. The big challenge of joining Mg/steel is the great difference of their melting points and the nearly zero inter-solubility between Mg and Fe [5], which causes many processing problems unless the heat input is well controlled.

Recently, solid state joining process, friction stir welding (FSW) was tried to join Mg alloy to steel [6–9]. Results show the good joining strength can be obtained, which reaches 70–80 % of the Mg substrate. Resistance spot welding (RSW) of AZ31B Mg alloy to Zn-coated steel also produced the joint strength as high as 95 % of that of Mg-Mg joint [10]. However, efficiency, flexibility and joining of three-dimensional complex structures are obstacles for FSW and RSW to meet the complicate production need of industries. As a non-contact joining technology, laser welding can overcome the problems above mentioned by combined with CNC working stage. Laser-GTA (gas tungsten arc) hybrid welding was first used to join Mg to stainless steel in lap configuration, but the results indicated poor joining strength and Mg-Fe interfacial fracture [11]. By inserting a nickel or copper interlayer, the shear strength of laser-GTA hybrid welded Mg/mild steel lap joints could be improved significantly [12]. Recently, a newly laser welding-brazing was developed to join dissimilar metals [13–15]. In this process, the metal with low melting point is fully melted by laser beam, while that with high melting point is un-melted or partially melted by controlling the quantity of heat input. Importantly, good joint of Mg to mild steel has been obtained by CO_2 laser welding-brazing, the maximum tensile strength of which reaches 185 MPa (about 82 % of AZ31B alloy) [16, 17]. Wahba and Katyama studied the laser lap welding of AZ31B magnesium alloy to Zn-coated steel, and also got high

*Corresponding author: tel.: +86 27 87792404; fax: +86 27 87541423; e-mail address: mgao@mail.hust.edu.cn

Table 1. Chemical composition (wt.%) of base metals

Element	Al	Zn	Mn	Si	Fe	Cu	Mg		
AZ31B	2.734	1.201	0.352	0.023	0.004	0.008	Bal.		
Element	C	Mn	P	S	Si	N	Ni	Cr	Fe
304 steel	0.070	2.000	0.045	0.030	0.075	0.100	9.253	18.25	Bal.

Table 2. Welding parameters and tensile results. The asterisk (×) indicates the joint directly fractures after welding. The UTS of AZ31B Mg alloy and 304 stainless steel are 235 and 546 MPa, respectively

Joint no.	Laser power P (kW)	Welding speed v (m min^{-1})	Laser offset δ (mm)	Heat input Q (J mm^{-1})	UTS (MPa)
# 1	2.0	1.5	0.1	80	×
# 2			0.2		×
# 3			0.3		142
# 4			0.4		89
# 5			0.5		×
# 6	2.5	3.0	0.1	50	×
# 7			0.2		211
# 8			0.3		169
# 9			0.4		×

tensile shear strength that exceeds 6 kN for a 25 mm wide joint [18]. However, no report has paid attention on laser welding of Mg to stainless steel in butt configuration.

This article aims to study the laser braze welding of AZ31B Mg alloy to 304 stainless steel by employing a fiber laser with high efficiency and excellent beam quality [19]. The interface characterization and fracture mechanisms of the joints are discussed to deepen the understanding.

2. Experimental procedure

A 6 kW fiber laser (IPG YLR-6000) with the wavelength of 1070 nm and a beam parameter product (BPP) of 6.9 mm mrad was employed. The laser beam was transmitted by a 200 μm core diameter fiber and focused by a 250 mm lens to get a spot size of 0.4 mm. The base materials were commercial 304 stainless steel with a thickness of 2 mm and commercial AZ31B-T5 Mg alloy sheets with a thickness of 3 mm. Since the Mg is easy to be vaporized by high temperature during welding, the thicker Mg sheet was used to avoid the underfill defect caused by the loss of Mg to get a full joint. Table 1 shows the chemical compositions of the two base metals.

Figure 1 shows the schematic diagrams of the experimental set-up. Square butt joints with 50×100 mm^2 rectangular plates were used and groove surfaces were machined and degreased with acetone. The laser

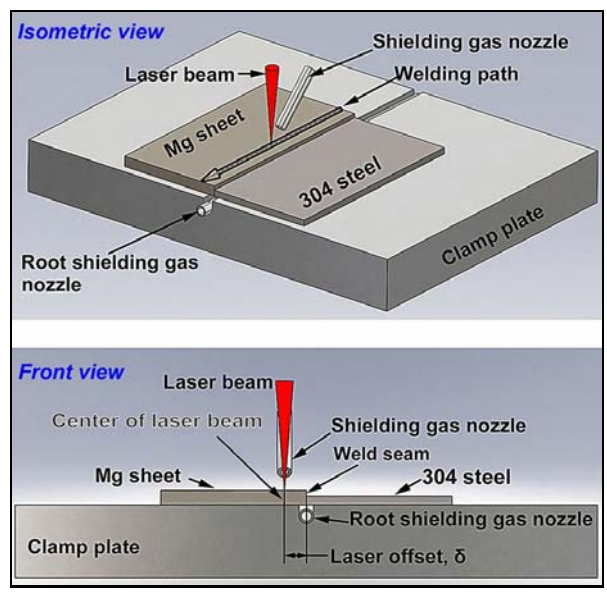

Fig. 1. Schematic diagram of experimental set-up.

welding-brazing parameters are shown in Table 2. The laser defocused distance is 0 mm, and the flowing rate of paraxial and root argon shielding gas were 10 and 7 l min^{-1}, respectively. As shown in Fig. 1, the laser beam irradiated on the Mg plate with an offset δ from the center of laser beam to the edge of joint seam.

After welding-brazing, specimens were cut midway from the joint, then polished and etched by a solution of 4.2 g picric acid, 10 ml acetic acid, 10 ml water and

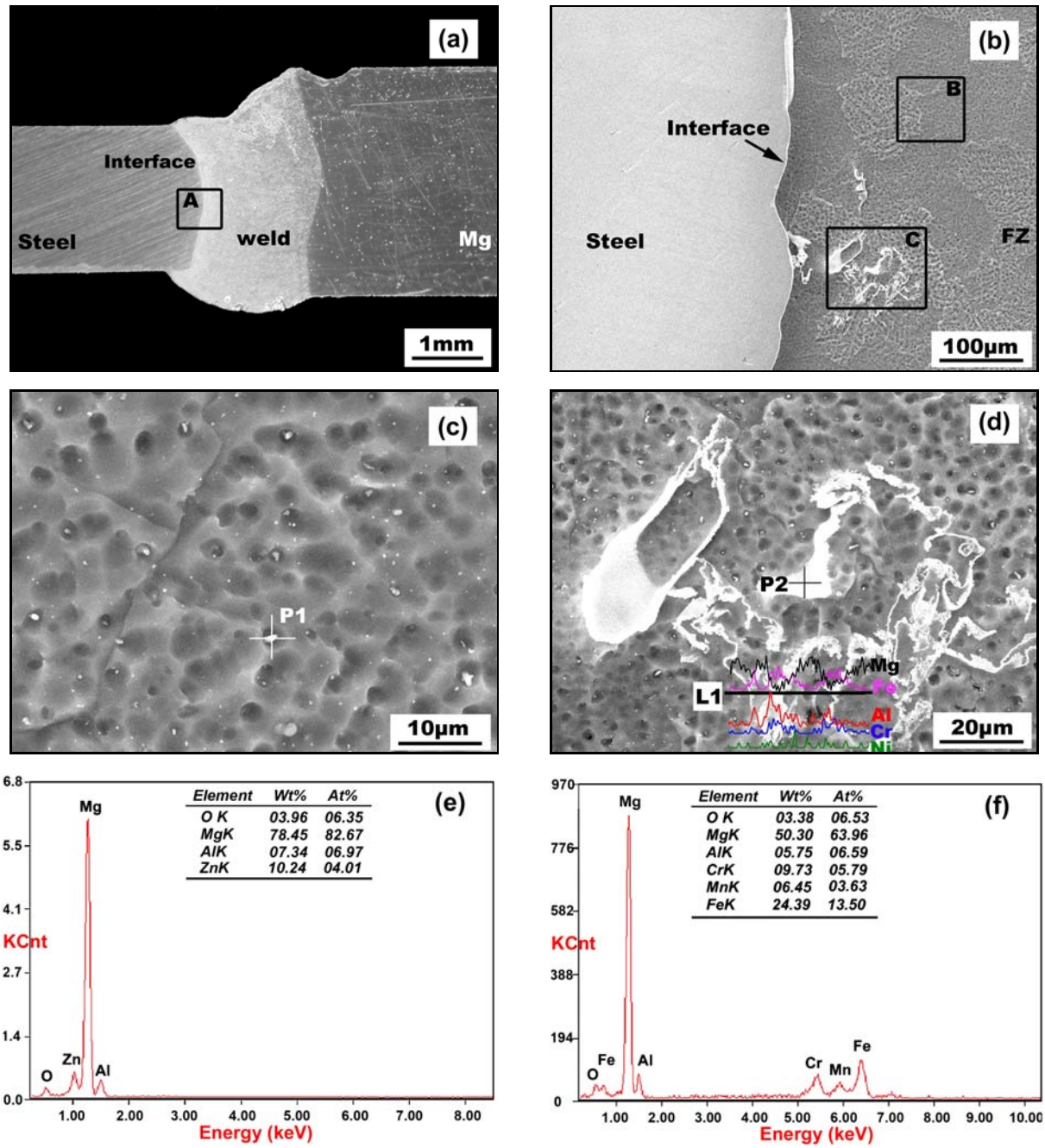

Fig. 2. Bead shape and microstructure of the joint # 7: (a) bead shape, (b) details of area A, (c) details of area B, (d) details of area C and EDS result of line L1, (e) EDS result of point P1, (f) EDS result of point P2.

100 ml ethanol. The microstructure and fracture surface were observed by SEM (scanning electron microscopy). The chemical compositions were examined by EDS (energy dispersive spectrometry) technique. The intermetallic compounds in the interface were tested by XRD (X-ray diffraction) technique. The rectangle sample with the size of 100×15 mm^2 was prepared for tensile test. The tensile test was carried out at room temperature and the result was the average of three samples cut from one joint.

3. Results and discussion

3.1. Microstructure and interface characterization

The joint cross-section morphologies in Fig. 2a,b show the steel/weld interface free of defects. The curve interface suggests the steel is melted during welding--brazing. As shown in Fig. 2b,c, the fusion zone (FZ) consists of massive α-Mg but contains some dispersed

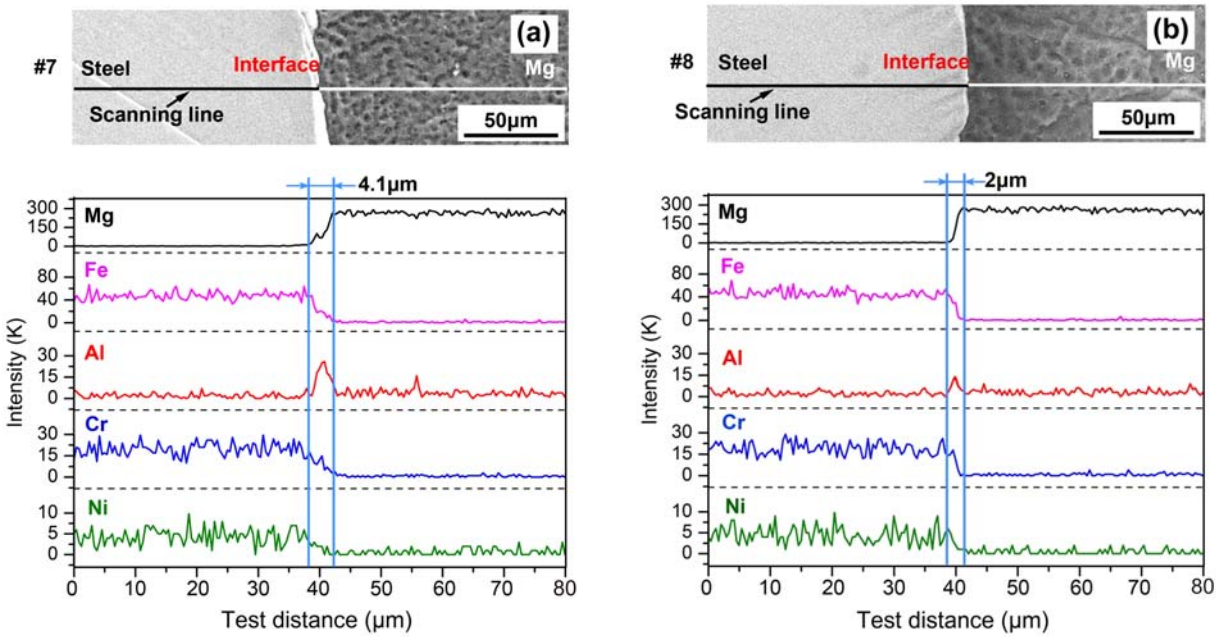

Fig. 3. EDS analysis of transition zone from steel to weld metal: (a) # 7 with $\delta = 0.2$ mm, (b) # 8 with $\delta = 0.3$ mm.

particles in α-Mg grains, which is a typical structure of AZ31B Mg fusion welds [20–22]. In Fig. 2d, some irregular white structures are observed near the interface. The EDS analysis results in Fig. 2e,f show that both the dispersed particles in α-Mg and the white structure are rich in alloying elements in comparison with Mg matrix. Hereinto, position P1 is rich in Al and Zn. During the solidification of molten pool, some of the Al atoms in the intermetallic compound $Mg_{17}Al_{12}$ can be replaced by Zn to form the $Mg_{17}(Al, Zn)_{12}$ at temperatures below 710 K [20, 23]. Therefore, the dispersed particles in α-Mg are identified as $Mg_{17}(Al, Zn)_{12}$. The EDS result of line L1 in Fig. 2d shows the white structure is rich in Fe, Cr and Ni, which come from stainless steel. Position P2 shows the white structure contains 24.39 wt.% Fe, 9.73 wt.% Cr, 6.45 wt.% Mn and 50.3 wt.% Mg. Obviously, the white structure is formed by the intermixing of melted 304 stainless steel with liquid Mg alloy in the molten pool. The small amount of O may come from the entrapment of air.

Figure 3 shows the element distributions of the transition zones with different laser offset. Elements Fe, Cr and Ni decrease but Mg increases gradually from the stainless steel to the weld metal. However, the Al concentration in the transition zone with the δ of 0.2 mm is more obvious than that with the δ of 0.3 mm. Since all the joints fracture in the steel/weld interface, XRD analysis on the fracture surface at steel side is used to indentify the intermetallic compounds in transition zone. As shown in Fig. 4, the intermetallic compounds of $Mg_{17}A_{12}$ and Mg_2Ni are observed, indicating that chemical reaction diffusion happens in the interface. The higher Al concentration suggests

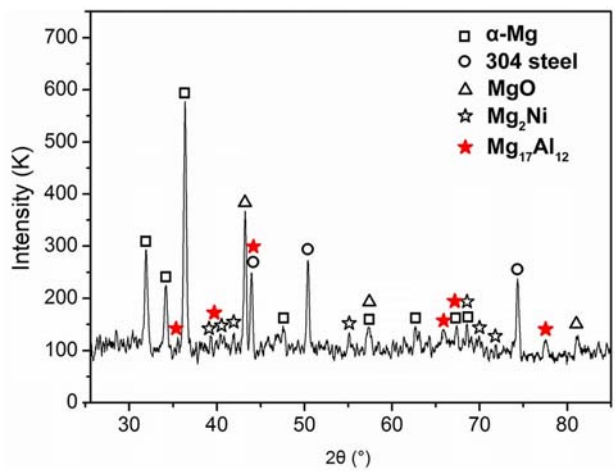

Fig. 4. XRD result on the fracture surface at steel side of joint # 7.

that stronger reaction diffusion occurs in the transition zone with smaller δ.

The other notable finding is that the thickness of transition zone increases by decreasing the δ. In Fig. 3, the thickness of the transition zone with $\delta = 0.2$ mm is about 4.1 μm, nearly double that with $\delta = 0.3$ mm (about 2.0 μm). It can be explained by the following diffusion mechanism. The appearance of the intermetallic compounds $Mg_{17}A_{12}$ and Mg_2Ni indicates that the reactive diffusion plays an important role in the formation of transition zone. Generally, the thickness of reactive diffusion layer along the interface is estimated by the following formula [16, 24]:

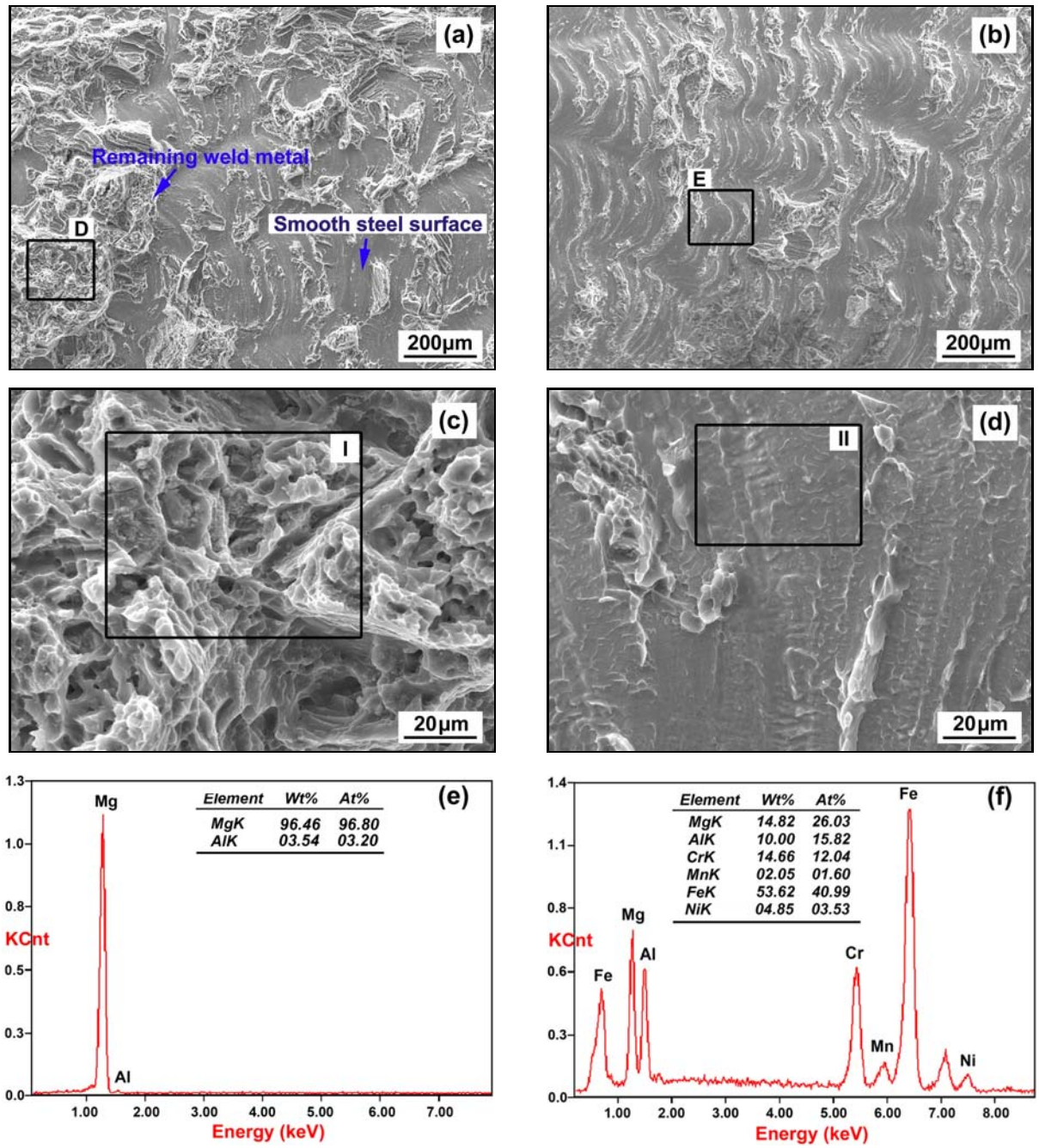

Fig. 5. Fracture surface at steel side of typical joints: (a) and (b) are the macro SEM morphologies of joint # 7 and # 8, respectively, (c) and (d) are the details of area D and E, respectively, (e) and (f) are the chemical EDS results of area I and II, respectively.

$$D = k_0 t^n \exp[-Q/(RT)], \quad (1)$$

where D is the thickness of transition zone, k_0 is a constant, t is the diffusion time, n is the time factor (~ 0.5), R is the gas constant, Q is the activation energy for layer growth and T is the absolute temperature at the interface. According to this formula, the thickness of transition zone increases with the interface temperature and/or the diffusion time. The interface temperature has two effects on the growth of transition zone. One is the thermal activation energy of atoms enhanced by increasing interface temperature, which leads to a higher diffusion coefficient to speed the growth of transition zone. The other is the solidification time (i.e., the diffusion time of the transition zone) of molten pool prolonged by increasing the interface temperature. Since reducing the laser offset indicates more heat is transferred to original Mg/steel interface by heat conduction and convection in molten pool, the smaller laser offset gets higher interface tem-

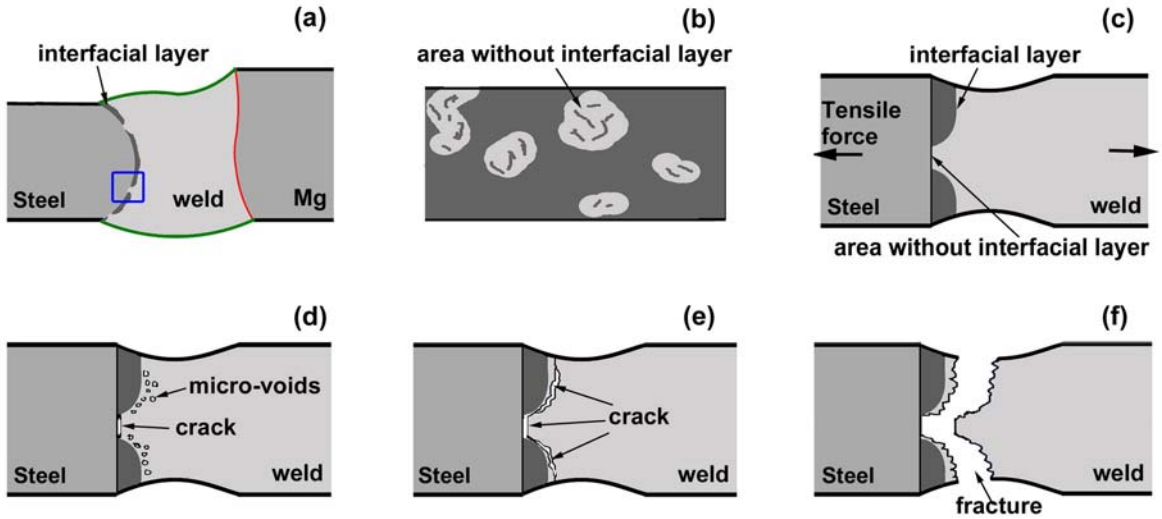

Fig. 6. Schematic diagram of fracture mechanisms: (a) cross-section of the interface, (b) distribution of reaction layer on the interface, (c) through (f) are the enlarged pictures of the rectangle area in (a) and refer to the fracture stages: (c) initial stage with necking, (d) micro-voids formation at the front of the reaction layer and crack at the area without reaction layer, (e) coalescence of micro-voids to form a crack and subsequent crack propagation, (f) final fracture morphology.

perature, and subsequently obtains a thicker interface.

3.2. Fracture behavior

In the tensile test, all the joints break at the interface of the FZ and stainless steel. For this reason, the ultimate tensile strength (UTS) was computed by the formula:

$$\sigma = F/A_0, \tag{2}$$

where σ is UTS, F is tensile force, A_0 is the cross-section area. The A_0 is calculated by the sample width and the thickness of steel plate due to the fracture in the interface.

Table 2 shows the data of joint UTS. The maximum UTS is up to 211 MPa, 89.8 % that of Mg substrate (235 MPa). Under the constant laser power and welding speed, the UTS strongly depends on δ, and increases with decreasing δ. It would be attributed to the bonding manner of the transition zone.

In Fig. 5a,b, the fracture surfaces at steel side are composed of scraggly and smooth areas, and the fraction of scraggly area to total surface increases with decreasing δ. As shown in Fig. 5c, the scraggly areas are characterized by ductile-brittle fracture characteristic, which consists of evident equiaxed dimple patterns and small amount of quasi-cleavage. It is similar to the typical fracture morphology of Mg welds [25, 26]. In Fig. 5e, the chemical composition of the scraggly area is similar with that of Mg substrate. Hence the scraggly areas shall be the Mg weld metal remaining on steel side. The low Al content (only 3.54 wt.%) of the remaining weld metal indicates the scraggly locations fracture at the weld metal close to the transition zone rather than in it owing to the transition zone with the intermetallic compound of $Mg_{17}Al_{12}$ has higher Al content. It also suggests that the transition zone with chemical reaction (reaction layer) has high joining strength because of the chemical bonding. As shown in Fig. 5d, the smooth areas belong to brittle fracture due to the plane morphologies and some shallow tearing ridges on the plane. Figure 5f shows that the smooth area mainly contains Fe element with a small quantity of Mg. Obviously, it is the steel surface but with little remaining weld metal. This observation suggests the smooth locations shall be lack of the reaction layer with chemical reaction. In these areas, the steel sheet and weld metal are only mechanically bonded by van der Waals force with poor joining strength. As a result, these areas crack at steel surface directly during tensile test.

As discussed above, the smaller δ means more areas of reactive layer forming on the interface due to higher interface temperature and longer diffusion time, which is also proved by the fracture characteristics in Fig. 5a,b. Consequently, the smaller δ leads to higher joining strength due to the larger area proportion of reaction layer to the whole interface.

According to above observation and discussion, the fracture mechanism of the joints can be drawn as follows. First, some locations are in lack of reaction layer as illustrated in Fig. 6a,b. At initial stage of tensile test, the big differences of the two base metals in elastic modulus and yield strength cause stress concentration at the interface, which deforms the 'soft' Mg weld metal firstly. It leads to a necking in the weld metal at the front of the reaction layer, as shown in Fig. 6c. Next, as shown in Fig. 6d, the locations without reaction layer crack directly. And the

cracks propagate rapidly to the locations with reaction layer by the tensile load. Meanwhile, some micro-voids form at the front of the reaction layer by the stress concentration. As the tensile load continues, these micro-voids enlarge, come together, and coalesce to form some large cracks along the reaction layer as shown in Fig. 6e. Finally, as shown in Fig. 6f, two kinds of cracks coalesce and break through the whole weld material to form the fracture surface.

4. Conclusions

Fiber laser welding-brazing was developed to join 304 stainless steel and AZ31B Mg alloy in butt configuration, and accepted joints with the maximum joining strength of 211 MPa, 89.8 % that of Mg substrate was obtained. A transition zone containing the intermetallic compounds of Mg_2Ni and $Mg_{17}Al_{12}$ are observed between the FZ and stainless steel. The thickness of transition layer increases by decreasing the laser offset. Moreover, the smaller the laser offset, the larger the area fraction of the reaction layer to whole interface and thus the stronger the joining strength. During the tensile test, the locations with reaction layer crack in the weld metal and are characterized by scraggly remaining Mg weld metal, while those without reaction layer crack at the steel surface directly and are characterized by smooth surface with some shallow tearing ridges.

Acknowledgements

The authors gratefully acknowledge the financial supports from the National Natural Science Foundation of China with grants no. 51275186 and 51128501.

References

[1] ASM Handbook: Properties and Selection Irons, Steels, and High-performance Alloys. New York, ASM International 1990.
[2] Friedrich, H. E., Mordike, B. L.: Magnesium Technology. Berlin, Springer 2006.
[3] Phanikumar, G., Chattopadhyay, K., Dutta, P.: Sci. Technol. Weld. Join., *16*, 2011, p. 313.
[4] Debroy, T., Bhadeshia, H. K. D. H.: Sci. Technol. Weld. Join., *15*, 2010, p. 266. doi:10.1179/174329310X12726496072400
[5] Liu, C. M., Zhu, X. R., Zhou, H. T.: Phase Diagrams of Magnesium Alloys. Changsha, Central South University Press 2006.
[6] Watanabe, T., Kagiya, K., Yanagisawa, A., Tanabe, H.: J. Jpn. Weld. Soc., *24*, 2006, p. 108. doi:10.2207/qjjws.24.108
[7] Jana, S., Hovanski, Y., Grant, G. J.: Metall. Mater. Trans. A, *41A*, 2010, p. 3173. doi:10.1007/s11661-010-0399-8
[8] Chen, Y. C., Nakata, K.: Mater. Des., *30*, 2009, p. 3913. doi:10.1016/j.matdes.2009.03.007
[9] Liyanage, T., Kilbourne, J., Gerlich, A. P.: Sci. Technol. Weld. Join., *14*, 2009, p. 500. doi:10.1179/136217109X456960
[10] Liu, L., Xiao, L., Feng, J. C., Tian, Y. H., Zhou, S. Q., Zhou, Y.: Metall. Mater. Trans. A, *41A*, 2010, p. 2651. doi:10.1007/s11661-010-0333-0
[11] Liu, L. M., Zhao, X.: Mater. Charact., *59*, 2008, p. 1279. doi:10.1016/j.matchar.2007.10.012
[12] Qi, X. D., Song, G.: Mater. Des., *31*, 2010, p. 605. doi:10.1016/j.matdes.2009.06.043
[13] Chen, Y. B., Chen, S. H., Li, L. Q.: Int. J. Adv. Manuf. Tech., *44*, 2009, p. 265. doi:10.1007/s00170-008-1837-2
[14] Gao, M., Mei, S. W., Wang, Z. M., Li, X. Y., Zeng, X. Y.: Sci. Technol. Weld. Join., *17*, 2012, p. 269. doi:10.1179/1362171812Y.0000000002
[15] Gao, M., Wang, Z. M., Li, X. Y., Zeng, X. Y.: Metall. Mater. Trans. A, *43A*, 2012, p. 163. doi:10.1007/s11661-011-0825-6
[16] Miao, Y. G., Han, D. F., Yao, J. Z., Li, F.: Sci. Technol. Weld. Join., *15*, 2010, p. 97. doi:10.1179/136217109X12518083193676
[17] Miao, Y. G., Han, D. F., Yao, J. Z., Li, F.: Mater. Des., *31*, 2010, p. 3121. doi:10.1016/j.matdes.2009.12.035
[18] Wahba, M., Katayama, S.: Mater. Des., *35*, 2012, p. 701. doi:10.1016/j.matdes.2011.10.031
[19] Quintino, L., Costa, A., Miranda, R., Yapp, D.: Mater. Des., *28*, 2007, p. 1231. doi:10.1016/j.matdes.2006.01.009
[20] Quan, Y. J., Chen, Z. H., Gong, X. S., Yu, Z. H.: Mater. Sci. Eng. A, *496*, 2008, p. 45. doi:10.1016/j.msea.2008.04.065
[21] Wang, Z. M., Gao, M., Tang, H. G., Zeng, X. Y.: Mater. Charact., *62*, 2011, p. 943. doi:10.1016/j.matchar.2011.07.002
[22] Chowdhury, S. M., Chen, D. L., Bhole, S. D., Powidajko, E., Wecjma, D. C., Zhou, Y.: Metall. Mater. Trans. A, *42A*, 2011, p. 1974. doi:10.1007/s11661-010-0574-y
[23] Czerwinski, F.: Acta Mater., *50*, 2002, p. 2639. doi:10.1016/S1359-6454(02)00094-0
[24] Song, W., Saida, K., Ando, A.: J. Jpn. Weld. Soc., *22*, 2004, p. 315. doi:10.2207/qjjws.22.315
[25] Gao, M., Mei, S. W., Wang, Z. M., Li, X. Y., Zeng, X. Y.: J. Mater. Process. Tech., *212*, 2012, p. 1338. doi:10.1016/j.jmatprotec.2012.01.011
[26] Gao, M., Tang, H. G., Chen, X. F., Zeng, X. Y.: Mater. Des., *42C*, 2012, p. 46. doi:10.1016/j.matdes.2012.05.034